# Diffraction waves on large aspect ratio rectangular submerged breakwaters

Esmaeel Masoudi[a,*], Lian Gan[a]

[a]*Department of Engineering, Durham University, United Kingdom*

**Abstract**

In this paper, hydrodynamic characteristics of two-dimensional submerged breakwaters in water of finite depth and infinite domain interacting with sinusoidal waves are studied from both analytical and numerical approaches. Added mass and damping coefficients are obtained following the determination of radiation potentials in three degrees of freedom (sway, heave and roll). Diffraction problem is then solved according to the linear wave theory and the resulting forces are derived. To verify the results, a comparison of the solution from the analytical method with those obtained by the boundary element method is made and a good agreement is observed. Additionally, high aspect ratio horizontal and vertical flat submerged breakwaters are proposed and their hydrodynamic characteristics are analyzed using the numerical and analytical methods. Results show that the horizontal flat submerged breakwater generates low transmitted waves. However, the vertical flat submerged breakwater transmits almost the entire incident wave energy. A parametric study on the effect of submergence depth and the width of the structure on the maximum diffraction wave amplitude, which is responsible for the transmitted wave energy, is carried out and a better understanding of the variation of diffraction wave amplitudes with respect to dominant parameters and wave frequency is achieved.

## 1. Introduction

The development of coastal or inland waters may often depend on sea behaviour at a specific site. Breakwaters of various dimensions and configurations have been widely employed to increase the use of locations exposed to wave attack. The main purpose of installing a breakwater is to reduce wave height to an acceptable level with respect to usage of the site. The increase in the number of private pleasure crafts and small vessels has engendered a demand for more sheltered sites. Affordability and required level of wave protection would often dictate possible breakwater alternatives. Rubble mound breakwaters have been widely used to attenuate surface water waves. In recent years, several floating breakwaters (FBs) are employed in coastal areas all over the world. Submerged breakwaters (SBs) were also a field of interest to many researchers. FBs and SBs usually consist of a floating pontoon with finite draft which are exposed to hydraulic waves. Motions of these breakwaters are usually constrained to three degrees of freedom. That is sway, heave and roll.

In the framework of numerical methods to study breakwater's performance in waves, finite element method (FEM) and boundary element method (BEM) are two popular and effective approaches which have been widely applied to breakwater performance analysis. As far as FEM and BEM are concerned, there are many published studies. As examples, Yamamoto et al. (1980) used BEM to solve two-dimensional problems of the response of the moored floating objects to water waves. They solved the boundary value prob-

*Corresponding author

*Email addresses:* esmaeel.masoudi@durham.ac.uk (Esmaeel Masoudi), lian.gan@durham.ac.uk (Lian Gan)

lem numerically by direct use of Green's identity formula for a potential function. Their results mostly focused on mooring configuration effects on wave attenuation characteristic of the floating body. Li et al. (1991) employed finite - infinite element method to obtain hydrodynamic exciting forces in regular waves. They utilized the inhomogeneous far field boundary conditions and the higher order asymptotic solutions to obtain second order diffraction forces and wave run-up profiles on a vertical cylinder. Their method showed better agreement with experimental results compared to the predictions from the linear theory. Sannasiraj et al. (1995) applied FEM to investigate the radiation and diffraction problem of a horizontal FB under the action of multi-directional waves. They evaluated wave exciting forces and relative induced responses using linear transfer-function approach for a rectangular cross section floating structure. The force and response ratio were also obtained in their study for frequency dependent-independent cosine power type directional spreading functions. Sannasiraj et al. (2001) also used the same finite element technique to study multiple floating structures. Wu and Taylor (2003) used coupled FEM and BEM, based on the combination of their strengths, to study nonlinear interactions between waves and bodies. They introduced auxiliary functions to decouple the mutual dependence of the body acceleration and hydrodynamic forces. Presenting their results for submerged circular and elliptical cylinder, they asserted that their numerical scheme could also be used for floating structures. Kunisu (2010) compared the results of BEM with those from experiments and studied the wave forces on a submerged floating tunnel. Evaluating exciting forces on a submerged circular cylinder using BEM as well as the well-known Morison's equation, they concluded that the inertia forces are dominant in large circular cylinders only when the Keulegan–Carpenter number is less than 15 for all incident wave frequencies. Chen et al. (2016) built FEM based Navier-Stokes equation and volume of fluid (VOF) method to investigate wave energy extraction by two-dimensional oscillating cylinders in linear waves for incompressible viscous flows. Based on wave climate off China's shore and building cost, they suggested that the cylinder diameter must be twice the incident wave height in order to obtain the best energy harvest efficiency. Zhan et al. (2017) applied zonal hybrid Reynolds averaged Navier-Stokes (RANS)/laminar method with a new meshing strategy to investigate hydrodynamic performance of an inverse T-type breakwater. They investigated heave and pitch transfer functions as well as transmission and reflection coefficients for floating and fixed breakwaters in regular and irregular waves. Tabatabaei and Zeraatgar (2018) utilized FEM for studying a moored pontoon type FB considering response amplitude operators (RAOs). They suggested that in spite of the fact that rectangular FBs are more commonly used in industry, circular FBs should also be considered for their better hydrodynamic performance in a wider range of incident wave frequencies. Masoudi (2019) employed BEM to study inverse T-type FB's hydrodynamic performance in sinusoidal waves. It was concluded that inverse T-type FB has lower transmission coefficient than rectangular FB over a wide range of incident wave frequencies and so could be considered for practical applications.

Analytical methods have also been used in many studies, some of which are mentioned next. Garrett (1970) discussed about the excitation of waves inside a partially immersed open circular cylinder. He considered incident plane wave expanded in Bessel functions and for each mode he formulated the problem in terms of the radial displacement on the cylindrical interface below the cylinder. He deduced that the phase of the solution is independent of depth and resonances are found at wave-numbers close to those of free oscillations in a cylinder extending to the bottom. Garrett (1971) also discussed scattering gravity waves by a circular cylinder in order to determine the horizontal and vertical forces as well as torques on a dock. He discussed that the phase of the solution is independent of depth and so may be obtained from an infinite set of real equations, which were solved numerically by Galerkin's method. Hulme (1982) derived added

mass and damping coefficients and wave force acting on a floating hemisphere oscillating in incompressible inviscid fluid. Wu and Taylor (1990) and Wu (1993) solved second order diffraction and radiation problems for a horizontal cylinder in finite water depth. They stated that for horizontal oscillation motion of the cylinder, the first-order potential is asymmetric but the second-order potential is symmetric. Berggren and Johansson (1992) presented hydrodynamic coefficients of a wave energy device consisting of a buoy connected to a submerged plate. Lee (1995) studied the heave radiation problem of a rectangular structure in which non-homogeneous boundary value problem is linearly decomposed into a homogeneous one. They showed that the presented solution satisfies the non-homogeneous boundary condition in a sense of series convergence. They also found that smaller structure submergence and larger structure width would result in larger waves, radiation added mass and damping coefficients. Hsu and Wu (1997) compared BEM with their analytical method for analyzing hydrodynamic coefficients of an oscillating rectangular structure with a side wall and concluded that the resonant behavior would appear when the clearance between the sidewall and the structure equals integer times of half wave length generated by the oscillating structure. Abul-Azm and Gesraha (2000) used an eigen-function expansion method to study a moored FB in oblique waves. They deduced that hydrodynamic performance of the pontoon type FB in wave reflection or transmission has a strong dependence on the relative dimension of the cross section, while dynamic properties mostly depend on inertial characteristic. Williams et al. (2000) proposed an appropriate Green's function to study hydrodynamic properties of a pair of long floating pontoon breakwaters of rectangular section restrained by linear symmetric moorings. They showed that wave reflection properties of twin pontoons depend strongly on their width, draft and spacing and the mooring line stiffness, while their excess buoyancy is of less importance. Zheng et al. (2004a,b) derived an analytical solution for radiation and diffraction problem of a rectangular buoy and presented extensive results from added mass and damping coefficients and the effect of sidewall. Masoudi and Zeraatgar (2016) employed the method of separation of variables, including eigen-function expansion method, in which radiation and diffraction problem is solved in three sub-domains in order to study hydrodynamic characteristics, such as added mass and damping coefficients as well as exciting forces, of a two-dimensional rectangular FB in water of finite depth and infinite domain. Deng et al. (2019) used a semi-analytical method to study hydrodynamic performance of a T-type FB. The effects of the height and setup position of vertical screen on the dynamic response and hydrodynamic characteristics of the breakwater are discussed. Mohapatra and Soares (2019) derived the three-dimensional Green's function and Fourier-type expansion formula for analyzing wave reflection by a rigid vertical wall with a floating and submerged elastic plate. They used linear structural response and thin plate theory to obtain hydroelastic response of the structure and concluded that mitigation of hydroelastic response of floating structures depends significantly on modes of oscillation, mooring stiffness, compressive force, rigidity and suitable positioning of the submerged horizontal flexible membrane.

Analytical solution is normally approached by dividing the whole domain to sub-domains and then approximating the velocity potentials in each sub-domain using orthogonal functions. After the boundary conditions are satisfied on the whole domain and on the common boundaries between sub-domains, the unknown coefficients in orthogonal functions are solved and the velocity potentials become explicit in sub-domains. Having determined the velocity potentials and wave characteristics on both sides of the breakwater body, the transmission and reflection coefficients are obtained. Although assumptions are usually involved for simplification reasons, the results are explicit.

High aspect ratio SBs which could be made by a simple flat thin plate of steel are expected to be good substitutes for other conventional type of breakwaters having larger volume of materials. The former could be moored using typical moor-

ings such as catenary lines by adding buoyancy aids to the structure. In this study, two types of two-dimensional rectangular high-aspect ratio flat SBs (horizontally and vertically) submerged in water of finite depth and infinite extent subjected to regular sinusoidal waves are analytically studied by solving the velocity potential equations using the separation of variables method. Similar to other analytical approaches, turbulence effect are neglected. The method of separation of variables is firstly verified by a typical conventional SB geometry Zheng et al. (2007). Additionally, BEM using ANSYS AQWA software is employed to solve diffraction and radiation problems for comparison. Next, hydrodynamic characteristics, including exciting forces as well as the reflection and transmission coefficients are analyzed. In particular, a parametric study on the main parameters e.g. submergence depth and the width of the breakwater are carried out in order to estimate their effects on the diffraction wave amplitude, which is a dominant parameter of the transmission coefficient. Finally, the establishment of the diffraction wave is discussed and its effect on hydrodynamic performance is concluded.

## 2. Method

For large breakwater length to the wavelength ratios, fluid is assumed to be incompressible, inviscid and irrotational. As such, the velocity potential $\phi$ satisfies the Laplace equation as shown in Equation (1). The velocity components and pressure can then be expressed by Equation (2) and Equation (3), respectively.

$$\nabla^2\phi = 0 \tag{1}$$

$$\frac{\partial\phi}{\partial x} = u, \qquad \frac{\partial\phi}{\partial y} = v, \qquad \frac{\partial\phi}{\partial z} = w \tag{2}$$

$$\frac{\partial\phi}{\partial t} + \frac{1}{2}\nabla\phi^2 + gz + \frac{P}{\rho} = 0, \tag{3}$$

where $u$, $v$ and $w$ are velocity components in $x$, $y$ and $z$ direction respectively. $P$ is the dynamic pressure, $\rho$ is water density and $g$ is the gravitational acceleration. Basic problem configuration of the breakwater and the coordinate system are shown in Figure 1. It is assumed that a linear wave with amplitude $A_i$ and angular frequency $\omega = 2\pi/T_i$ propagates in a direction at an angle $\theta$ to the $+x$ axis. The total potential $\phi$ is composed of incident wave potential $\phi_i$, diffraction potential $\phi_d$, and radiation potentials $\phi_r$. The incident wave potential for a regular sinusoidal wave can be written as $\phi_i = \varphi_i(x,z)\exp(jky\sin\theta)$, in which:

$$\varphi_i = -\frac{jgA_i}{\omega}\frac{\cosh[k(z+h_1)]}{\cosh(kh_1)}\ \exp(jkx\cos\theta) \tag{4}$$

where $k$ is the wave number, $j$ represents unit imaginary number and $h_1$ is the depth of water. Also

$$\omega^2 = gk\tanh(kh_1) \tag{5}$$

is known as the *dispersion equation*. The diffraction potential $\phi_d$ is induced by the interaction of incident wave and the breakwater. The induced potential from the motions of structure in three degrees of freedom are known as radiation potential $\phi_r$.

Referring to Figure 1, the problem is considered as two-dimensional. That is, motions are restricted in heave, sway and roll, denoted as indices 1, 2 and 3, respectively. Hence the total potential $\phi_t$ could be expressed as:

$$\phi_t = \phi_i + \phi_d + \sum_{L=1}^{3}\phi_r^L \tag{6}$$

where $L$ refers to the assigned motion number and $\phi_r^L$ is the radiation potential of the $L^{th}$ motion. The unknown terms in the above equation are $\phi_d$ and $\phi_r^L$ which will be addressed next.

*The diffraction term $\phi_d$*

The linear diffraction term and its boundary conditions can be expressed by the oscillatory function

$$\phi_d(x,z,y) = \varphi_d(x,z)\ \exp(jky\sin\theta) \tag{7}$$

$$\frac{\partial\varphi_d}{\partial z} - \frac{\omega^2}{g}\varphi_d = 0\ \ (z=0\ ) \tag{8}$$

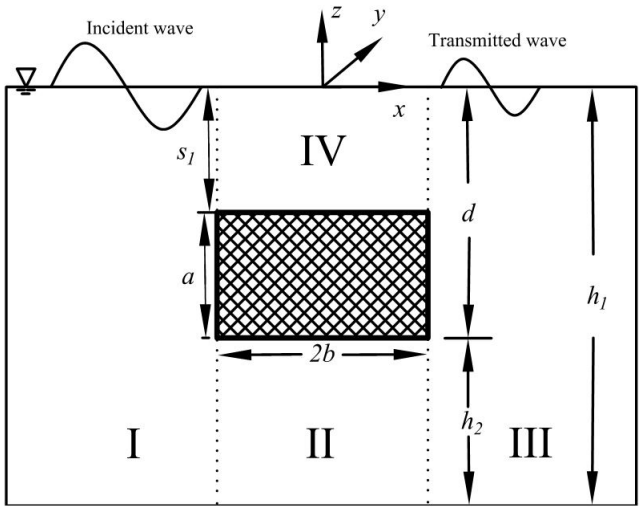


Figure 1: Problem configuration and coordinate system for a two-dimensional rectangular SB.

$$\frac{\partial \varphi_d}{\partial z} = 0 \ \ (z = -h_1) \tag{9}$$

$$\frac{\partial \varphi_d}{\partial n} = -\frac{\partial \varphi_i}{\partial n} \quad (\text{on } S_0) \tag{10}$$

$$\lim_{x\to\infty}\left[\frac{\partial \varphi_d}{\partial x} \pm jk\cos\theta\ \varphi_d\right] = 0 \tag{11}$$

The boundary value for the diffraction potential is defined by the governing Laplace equation and the boundary conditions are defined from Equation (8) to Equation (11), where $n$ is the unit normal vector outward the body surface and $S_0$ is the wetted surface of the breakwater.

*The radiation term $\phi_r^L$*

In the framework of the linear theory, the radiation term and its boundary conditions can also be described by the following oscillatory radiation potential and boundary conditions.

$$\phi_r^L(x,z,y) = -j\omega A_r^L\ \varphi_r^L\ (x,z)\ \exp(jky\sin\theta) \tag{12}$$

$$\frac{\partial \varphi_r^L}{\partial z} - \frac{\omega^2}{g}\ \varphi_r^L = 0 \ \ (z = 0) \tag{13}$$

$$\frac{\partial \varphi_r^L}{\partial z} = 0 \ \ (z = -h_1) \tag{14}$$

$$\frac{\partial \varphi_r^L}{\partial z} = \delta_{1,L} - (x - x_0)\delta_{3,L} \quad (z = -s_1 \ \ or\ z = -d\ , |x| \le b) \tag{15}$$

$$\frac{\partial \varphi_r^L}{\partial x} = \delta_{2,L} + (z - z_0)\delta_{3,L} \quad (-d \le z \le -s_1 \ \ , |x| = b) \tag{16}$$

$$\lim_{x\to\infty}\left[\frac{\partial \varphi_r^L}{\partial x} \pm jk\cos\theta\ \varphi_r^L\right] = 0 \tag{17}$$

where

$$\delta_{x,y} = \begin{cases} 1 & x = y \\ 0 & x \neq y \end{cases} \tag{18}$$

The amplitude of the $L^{th}$ motion of the body is denoted by $A_r^L$ and $(x_0, z_0)$ is the body centroid. The boundary value can be defined by Equation (1) and the boundary conditions are defined from Equation (13) to Equation (17).

*Separation of Variables Method*

Referring to Figure 1 the domain is divided into four sub-domains denoted by I, II, III and IV. Applying the separation of variables method gives the complex spatial potentials in each sub-domain expressed in terms of orthogonal series as below (Zheng et al., 2007). For the diffraction term,

velocity potentials are given from Equation (19) to Equation (22) for regions I to IV, respectively.

$$\varphi_{d_1} = \sum_{n=1}^{\infty} A_{1n}^{'} \, e^{-\gamma_n(x-b)} \, \cos[\lambda_n \, (z+h_1)] \quad (19)$$

$$\varphi_{d_2} = -\varphi_i + \sum_{n=1}^{\infty} [A_{2n}^{'} \, e^{\mu_n(x+b)} + B_{2n}^{'} \, e^{-\mu_n(x-b)}] \, \cos[\beta_n \, (z+h_1)] \quad (20)$$

$$\varphi_{d_3} = \sum_{n=1}^{\infty} A_{3n}^{'} \, e^{\gamma_n(x+b)} \, \cos[\lambda_n \, (z+h_1)] \quad (21)$$

$$\varphi_{d_4} = -\varphi_i + \sum_{n=1}^{\infty} [A_{4n}^{'} \, e^{\upsilon_n(x+b)} + B_{4n}^{'} \, e^{-\upsilon_n(x-b)}] \, \cos[\alpha_n \, (z+s_1)] \quad (22)$$

For the radiation term, velocity potentials are given from Equation (23) to Equation (26) for regions I to IV, respectively.

$$\varphi_{r_1}^{L} = \sum_{n=1}^{\infty} A_{1n}^{L} \, e^{-\gamma_n(x-b)} \, \cos[\lambda_n \, (z+h_1)] \quad (23)$$

$$\varphi_{r_2}^{L} = \varphi_{r_{2p}}^{L} + \sum_{n=1}^{\infty} [A_{2n}^{L} \, e^{\mu_n(x+b)} + B_{2n}^{L} \, e^{-\mu_n(x-b)}] \, \cos[\beta_n \, (z+h_1)] \quad (24)$$

$$\varphi_{r_3}^{L} = \sum_{n=1}^{\infty} A_{3n}^{L} \, e^{\gamma_n(x+b)} \, \cos[\lambda_n \, (z+h_1)] \quad (25)$$

$$\varphi_{r_4}^{L} = \varphi_{r_{4p}}^{L} + \sum_{n=1}^{\infty} [A_{4n}^{L} \, e^{\upsilon_n(x+b)} + B_{4n}^{L} \, e^{-\upsilon_n(x-b)}] \, \cos[\alpha_n \, (z+s_1)] \quad (26)$$

In the equations above, eigenvalues $(\gamma_n, \mu_n, \beta_n, \lambda_n, \upsilon_n, \alpha_n)$ are given by:

$$\lambda_1 = -jk, \; k\tanh(kh_1) = \frac{\omega^2}{g} \quad n = 1 \quad (27)$$

$$\lambda_n \tan(\lambda_n h_1) = -\frac{\omega^2}{g} \;\; n = 2, 3, \ldots \quad (28)$$

$$\alpha_1 = -jk_1, \; k_1\tanh(k_1 s_1) = \frac{\omega^2}{g} \quad n = 1 \quad (29)$$

$$\alpha_n \tan(\alpha_n s_1) = -\frac{\omega^2}{g} \quad n = 2, 3, \ldots \quad (30)$$

$$\beta_n = \frac{(n-1)\pi}{h_1 - d} \quad n = 1, 2, 3, \ldots \quad (31)$$

$$v_n = \begin{cases} -j\sqrt{k_1^2 - k_0^2} & n = 1 \\ \sqrt{\alpha_n^2 + k_0^2} & n = 2, 3, ... \end{cases} \quad (32)$$

$$\gamma_n = \begin{cases} jk\cos\theta & n = 1 \\ \sqrt{\lambda_n^2 + k_0^2} & n = 2, 3, ... \end{cases} \quad (33)$$

$$\mu_n = \begin{cases} k_0 & n = 1 \\ \sqrt{\beta_n^2 + k_0^2} & n = 2, 3, ... \end{cases} \quad (34)$$

Furthermore, in Equation (24) and Equation (26), $\varphi_{r_{2p}}^{L}$ and $\varphi_{r_{4p}}^{L}$ are particular solutions for the $L^{th}$ radiation motion in sub-domain II and IV, respectively, which are given by Zheng et al. (2007) as follows.

$$\varphi_{r_{2p}}^{L} = C_{F2}(z) \, [\delta_{1,L} - (x - x_0)\delta_{3,L}] \quad (35)$$

$$\varphi_{r_{4p}}^{L} = C_{F4}(z) \, [\delta_{1,L} - (x - x_0)\delta_{3,L}] \quad (36)$$

where:

$$C_{F2}\,(z) = \frac{\cosh[\mu_1 \, (z+h_1)]}{\mu_1 \, \sinh(\mu_1 \, h_2)} \quad (37)$$

$$C_{F4}\,(z) = \frac{\dfrac{\omega^2}{g}\,\sinh(k_0 z) + k_0\,\cosh(k_0 z)}{k_0\,\dfrac{\omega^2}{g}\,\cosh(k_0 s_1) - k_0\,\sinh(k_0 s_1)} \tag{38}$$

The potentials given from Equation (19) to Equation (26) describe the fluid in each region and satisfy all boundary conditions except the common boundaries between the regions. Now, the problem is to evaluate unknown coefficients $A^L_{1n}$, $A^L_{2n}$, $A^L_{3n}$, $A^L_{4n}$, $B^L_{2n}$, $B^L_{4n}$ for the radiation term and $A^{'}_{1n}$, $A^{'}_{2n}$, $A^{'}_{3n}$, $A^{'}_{4n}$, $B^{'}_{2n}$ and $B^{'}_{4n}$ for the diffraction term in the series. It should be noted that each coefficient has a unit which depends on the respective motion in the radiation term. These coefficients are found by imposing the boundary conditions that are the pressure continuity and normal velocity at the common boundaries between the regions, which are $x = \pm a$ and $0 < z < -s_1$, $-s_1 < z < -d_1$ and $-d_1 < z < -h_1$. In mathematical terms, it means that potentials and their normal derivatives are equal at boundaries. Satisfying these boundary conditions form a system of 6 linear equations which need to be solved simultaneously. To solve these equations, the orthogonal functions must be truncated. If $n$ is truncated to $N$ from Equation (19) to Equation (26), imposing the boundary conditions in the common boundaries will lead to a system of $6 \times N$ linear equations and equal number of unknown coefficients. Organizing these coefficients in matrices gives

$$S \cdot X = F \tag{39}$$

in which $X$ is the unknown coefficient matrix. There are three radiation and one diffraction potentials included in Equation (39). It should be noted that $S$ is a $6N \times 6N$ matrix which is obtained from satisfying the boundary conditions from Equation (8) to Equation (11) for diffraction and from Equation (13) to Equation (17) for radiation term. $F$ is a $1 \times 6N$ matrix which is obtained from satisfying the common boundary conditions between the regions and $X$ is a $M \times 6N$ matrix, in which $M$ is the total number of wave frequencies to solve according to the range and frequency increments. The detail of this method, including the calculation of $F$ is discussed in Masoudi and Zeraatgar (2016). Having known $F$ and $S$, $X$ is obtained for each of the four potentials. Finally, imposing the coefficients in Equation (19) to Equation (26), the velocity potentials for each region will be obtained.

*Expressions for Hydrodynamic Coefficients and Wave Forces*

If we denote the wave force perpendicular to the incident wave as $F_{w_u}$, which is independent of $y$ and time, it can be calculated from the incident and diffracted wave potentials as

$$F_{w_u} = \rho j\omega \int_{S_0} (\varphi_d + \varphi_i)\, n_u \,\mathrm{d}s \tag{40}$$

in which $n_u$ is the generalized inward normal to the structure in $x-z$ plane with $n_1 = n_z$, $n_2 = n_x$ and $n_3 = (z - z_0)n_x - (x - x_0)n_z$ with $n_x$ and $n_z$ being the unit inward normal to the surface of the body. Also, $CF_u$ is the exciting force coefficient which is a non-dimensional form of $F_{w_u}$ given by:

$$CF_u = \begin{cases} \dfrac{|F_{w_u}|}{2\rho b d A_i} & u = 1, 2 \\ \dfrac{|F_{w_u}|}{2\rho b^3 d A_i} & u = 3 \end{cases} \tag{41}$$

The hydrodynamic coefficients including the added mass coefficient $m_{L,u}$ and the damping coefficient $N_{L,u}$ are defined by

$$m_{L,u} = \rho \int_{S_0} \mathrm{Re}(\varphi^L_r\,)\, n_u\, ds \tag{42}$$

$$N_{L,u} = \rho \int_{S_0} \mathrm{Im}(\varphi^L_r\,)\, n_u\, ds \tag{43}$$

Also, $C_{m_u}$ and $C_{d_u}$ are the non-dimensional added mass and damping coefficients.

$$C_{m_u} = \begin{cases} \dfrac{m_{u,u}}{2\rho b d} & u = 1, 2 \\ \dfrac{m_{u,u}}{2\rho b^3 d} & u = 3 \end{cases} \tag{44}$$

$$C_{d_u} = \begin{cases} \dfrac{N_{u,u}}{2\rho\omega b d} & u = 1, 2 \\ \dfrac{N_{u,u}}{2\rho\omega b^3 d} & u = 3 \end{cases} \tag{45}$$

Transmission coefficient ($T_w$) is defined as the amplitude of the transmitted wave to the amplitude of the incident wave. Reflection coefficient ($R_w$) is defined as the amplitude of the reflected wave to the amplitude of the incident wave. If breakwaters are assumed to be stationary, using linearised Bernoulli equation, Zheng et al. (2007) obtained transmission and reflection coefficients

$$T_w = |\frac{j\omega A_{31}^{'} \cosh(kh_1)}{gA_i}| \tag{46}$$

$$R_w = |1 + \frac{j\omega A_{11}^{'} \cosh(kh_1)}{gA_i \exp(jkb\cos\theta)}| \tag{47}$$

Longuet-Higgins (1977) proposed the horizontal drift force ($F_d$) in terms of the reflection coefficient as

$$F_d = \left(\frac{Ec_g}{c}\right)(1 + R_w^2 - T_w^2) = \left(\frac{2Ec_g}{c}\right) R_w^2 \tag{48}$$

where $c_g$ is the wave group velocity, $c$ is the phase velocity, $E = \frac{1}{2}\rho g {A_i}^2$ is the wave energy. The added mass and damping coefficients will be evaluated using Equation (44) and Equation (45), respectively. The exciting force coefficients will be addressed using Equation (41). The transmission and reflection coefficients could be evaluated using Equation (46) and Equation (47) for the analytical and Equation (48) for the numerical method.

## 3. RESULTS

Based on the formulation discussed in section 2, Equation 39 is solved in MATLAB® with inputs being $\theta$, $a$, $b$, $h_1$, $h_2$, $s_1$, $d$, $A_i$ and the number of truncated terms in the orthogonal series being $N = 12$.

The solution is the unknown coefficients in orthogonal series which determine the velocity potentials for the diffraction and radiation terms according to Equation (19)-(26). Hydrodynamic characteristics of the domain are then evaluated using Equation (40)-(47). In order to verify the analytical method, a rectangular SB of $s_1/h_1 = 0.2$, $a/h_1 = 0.2$, $h_1/b = 6$, $\theta = 30^\circ$ is considered. The model characteristic has been chosen similar to Zheng et al. (2007) for validation purposes. Furthermore, a BEM numerical simulation using ANSYS AQWA is carried out for comparison. Figure 2 demonstrates the added mass coefficient ($C_m$), the damping coefficients ($C_d$), and the exciting force coefficients ($CF$) of the proposed breakwater. These are compared with Zheng et al. (2007). Evidently, all results are in reasonable agreement. The divergence between numerical and analytical results are thought to originate from converting three-dimensional results to two-dimensional quantities in numerical simulation. It should be emphasized that in analytical solution, the length of the breakwater mathematically assumed to be infinite, however, in numerical simulation the length of the breakwater considered to be 50 m. Table (1) summarises the model characteristics of the geometry, environmental constants, mass properties and mesh parameters for the numerical model. It should be noted that de-featuring tolerance controls how small details are treated by the mesh in AQWA. If any detail in the structure is smaller than this tolerance, a single element may span over it, otherwise the mesh size will be reduced in this area to ensure that the feature is meshed. In AQWA the maximum element size is explicitly related to the maximum wave frequency that can be utilized in the diffraction analysis. If a particular maximum wave frequency is desired, this can be specified as *maximum allowed frequency* and the associated maximum element size will be computed. In this study, after testing a number of maximum element size, the nearest value to the desired frequency range ($f_i \approx 0 - 0.4\ Hz$) is chosen. Desired frequency range is calculated according to the dispersion equation (Equation 5) with respect to the desired wave number which covers a range of response similar to Zheng et al. (2007). It should be emphasized that for the radiation term, according to Equation (44) and Equation (45), $C_m$ and $C_d$ are independent of incident wave amplitude. However for the diffraction term and for the evaluation of $C_F$, according to Equation (41), it is assumed that $A_i = 1m$.

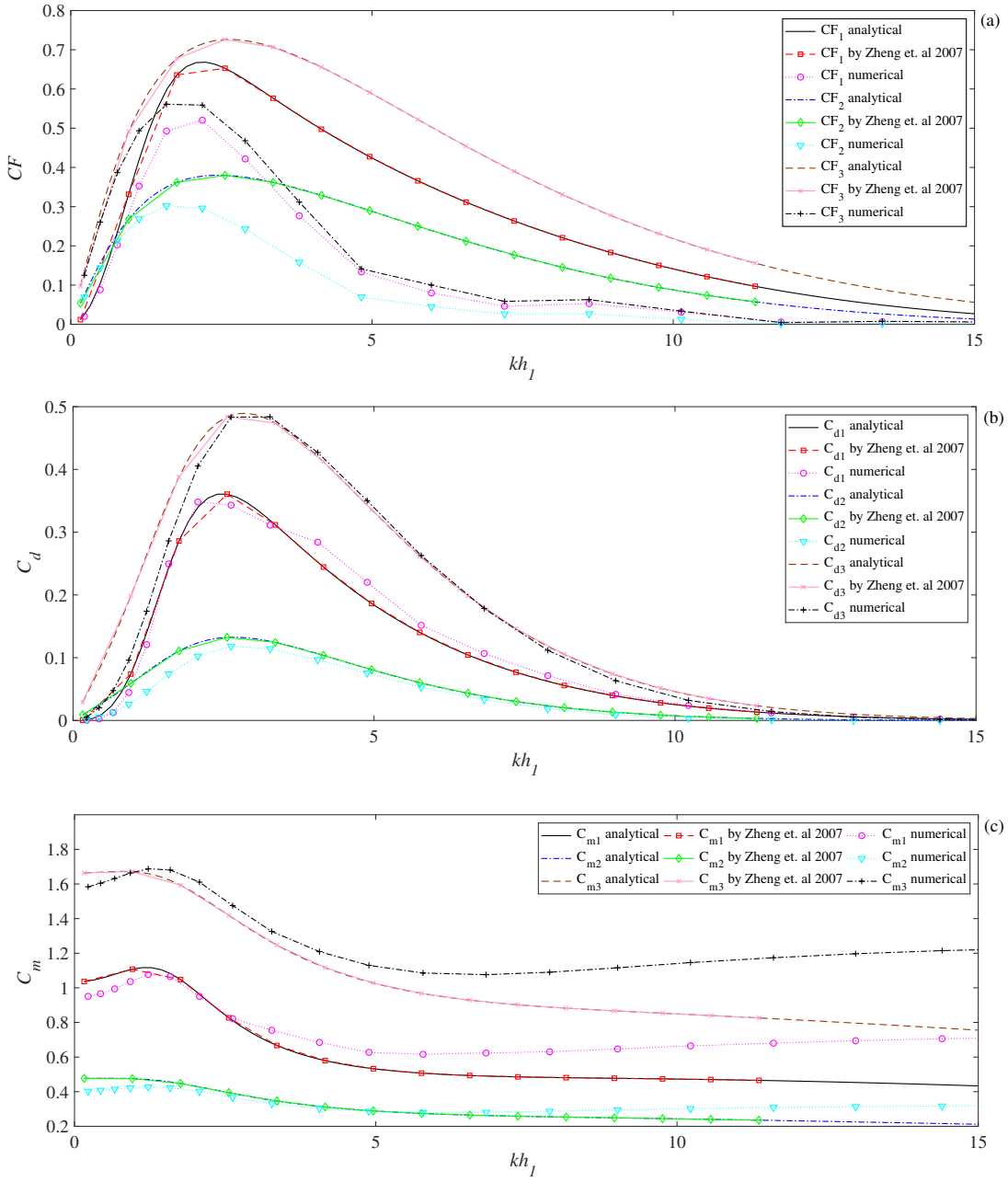


Figure 2: Comparison of numerical and analytical study on (a) exciting forces $CF_u$ (b) damping coefficients $C_{d_u}$ and (c) added mass coefficients $C_{m_u}$ of heave ($u = 1$), sway ($u = 2$) and roll ($u = 3$) motions/directions ($s_1/h_1 = 0.2,\ a/h_1 = 0.2,\ h_1/b = 6,\ \theta = 30°$)

*Horizontal and Vertical Flat SBs*

Two types of high aspect ratio SBs are studied in this work and their configurations are presented in Figure 3. The first one is denoted as a horizontal flat breakwater and the second one as vertical.

Figure 4 displays the exciting force coefficients, as defined in Equation (41), of horizontal and vertical flat SBs at conditions $s_1/h_1 = 0.1,\ \theta = 1°$. In the present analytical method, $\theta = 0°$ is a singular condition, hence $\theta = 1°$ is considered instead. Analytical and numerical methods are depicted simultaneously and reasonable agreement between the two is evident.

According to Equation (48), the mean drift force on the body can be calculated. The trans-

Table 1: Breakwater specifications, environmental constants and mesh parameters for numerical simulation

| **Geometry** | | **Environmental Constants** | |
|---|---|---|---|
| Length ($y$) | 50 $m$ | Water Depth | 48 $m$ |
| Width ($x$) | 16 $m$ | Water Density | 1025 $kg/m^3$ |
| Depth ($z$) | 9.6 $m$ | Gravity | 9.8 $m/s^2$ |
| **Mass Properties** | | Water Size $x$ | 1000 m |
| $x_0$ | 0 $m$ | Water Size $y$ | 1000 $m$ |
| $y_0$ | 0 $m$ | **Mesh Parameters** | |
| $z_0$ | -14.4 $m$ | De-featuring Tolerance | 1 $m$ |
| Mass | 15744 $t$ | Maximum Element Size | 2 $m$ |
| $K_{xx}$ | 29 $m$ | Maximum Allowed Frequency | 0.431 $Hz$ |
| $K_{yy}$ | 5.4 $m$ | Total Nodes | 3922 |
| $K_{zz}$ | 29.2 $m$ | Total Elements | 3920 |

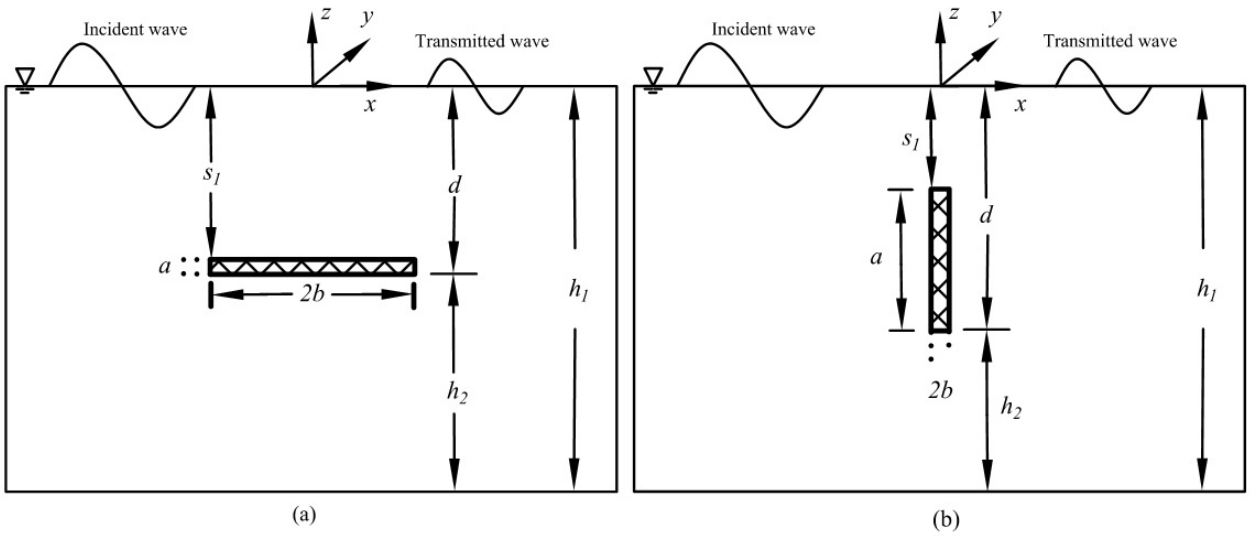


Figure 3: Basic configuration and coordinate system for (a) horizontal and (b) vertical flat SBs

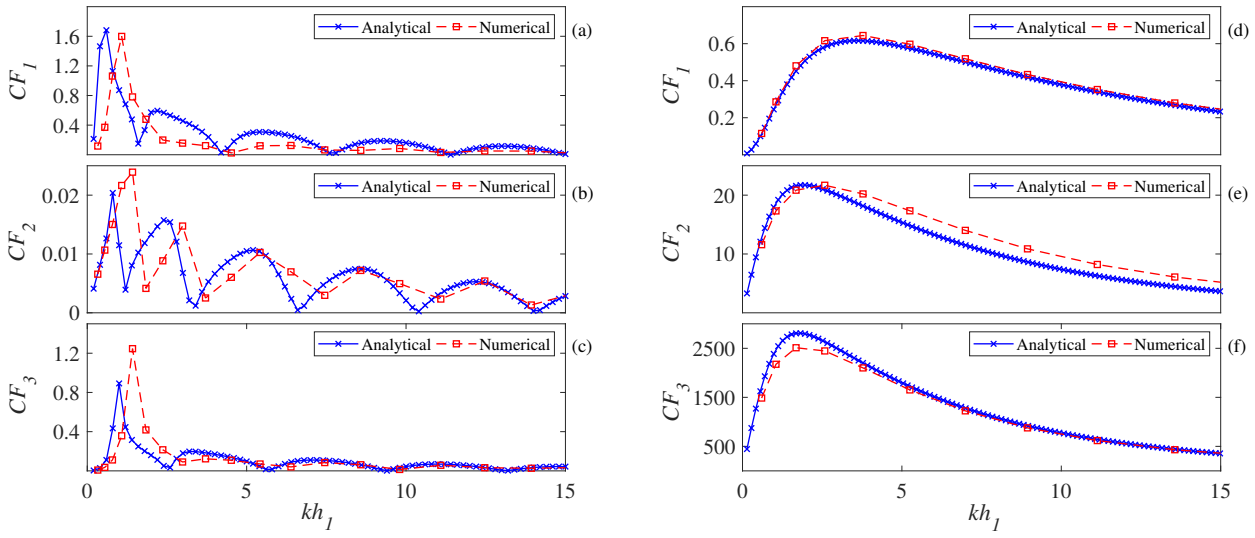


Figure 4: Exciting force coefficients for horizontal (a,b,c) and vertical (d,e,f) flat SBs ($s_1/h_1 = 0.1,\ \theta = 1°$)

mission and reflection coefficients can then be derived and the results are shown in Figure 5 for the vertical and the horizontal flat SBs of $s_1/h_1 = 0.1,\ \theta = 1°$. It should be noted that for the cases under consideration in Figure 3, the horizontal flat SB has a ratio $2a/b = 100$ and for the vertical flat SB, $2a/b = 0.01$.

## 4. DISCUSSION

Figure 4 shows that exciting force coefficient $CF$, which represents the combined effect of the incident and diffraction forces, oscillates as a function of wave number. Exciting forces for the horizontal flat breakwater are shown in Figure 4 (a,b,c) and that for the vertical flat breakwater are shown in Figure 4 (d,e,f). For the horizontal flat breakwater (a,b,c), exciting force coefficient varies both globally and locally with respect to the dimensionless wave number ($kh_1$). Globally, as the incident wave frequency increases, the force decreases quickly. Local oscillation can also be seen. It causes $CF_u$ to drop to zero at multiple wave numbers with an appeared phase lag from $CF_1$ to $CF_3$. For large wave numbers, $CF_u$ approaches to zero globally. The exciting force coefficient of the sway motion, $CF_2$, is much smaller in magnitude than $CF_1$ (heave) and $CF_3$ (roll). Note the different ordinate scales. Physically this is owing to the smaller projected area in the sway direction for the horizontal flat breakwater. Discrepancies between analytical and numerical results can be observed, which could be a result of converting three-dimensional analysis to two-dimensional quantities in numerical method.

The behaviour of the exciting force associated with the vertical flat breakwater (d,e,f) appears to be very different. Although they also display a global decay as $kh_1$ increases, no local oscillation is observed. This is believed to be due to diffraction force, which is mainly responsible for the oscillatory force behaviour, having negligible magnitude. The very large exciting force coefficient of the roll motion, $CF_3$, is related to the large projected area of the breakwater in the roll direction. It thus suggests that the vertical geometry has a high tendency to roll.

Figure 5 demonstrates transmission and reflection coefficients for both horizontal flat and vertical flat breakwaters using numerical method. It can be seen from the behaviour of $T_w$ and $R_w$ that the vertical flat breakwater almost transmits the entire incident wave energy (no reflects). On the contrary, the horizontal flat breakwater effectively attenuates incident wave energy especially for low wave numbers over the range $1 < kh_1 < 3$, in which transmission coefficient $T_w$ reaches the minimum value $\approx 0.4$ and $R_w$ reaches the maximum value of $\approx 0.84$. Those are considerable values comparing to conventional low aspect ratio SB.

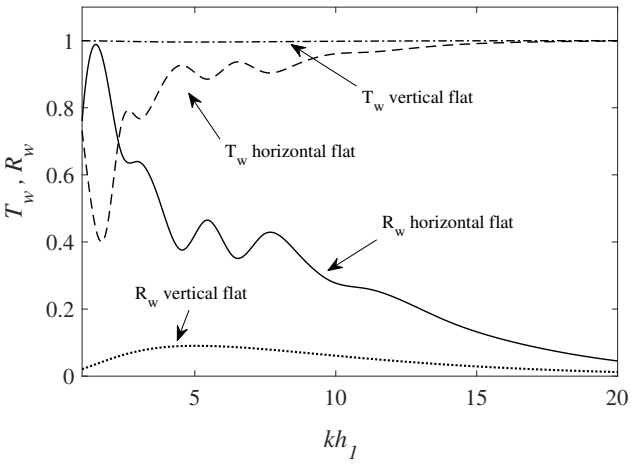


Figure 5: Transmission and reflection coefficient comparison of horizontal and vertical flat SBs ($s_1/h_1 = 0.1,\ \theta = 0$)

An oscillatory behaviour can also be seen for $T_w$ and $R_w$ for the horizontal flat breakwater, which is a direct reflection of the oscillatory diffraction force shown in Figure 4 (a,b,c). Additionally, no oscillatory behaviour is observed for vertical flat breakwater's $T_w$ and $R_w$, which is in consistence with the exciting force in Figure 4 (d,e,f). It is plausible that diffraction wave formation on the vertical and the horizontal flat breakwater is the basic reason for the large difference in their transmission coefficient behaviours. The large size in the $x$ direction of the horizontal flat breakwater leads to a lower transmission coefficient, as has been the main parameter in many previous FB studies. Additionally, it suggests that the breakwater's dimension in the incident wavelength direction plays the dominant role in

the performance of SBs as well as FBs.

In order to determine the effect of submergence depth on the reflection and transmission coefficients of the horizontal flat SB, Figure 6 is presented. First of all, as $s_1/h_1$ increases, the reflection coefficient $R_w$ decreases and the transmission coefficient $T_w$ increases. For $s_1/h_1 = 0.2$ the $T_w$ reaches a minimum value of 0.75 at $kh_1 \approx 2.5$, which means 75% of incident wave energy is transmitted from the breakwater. Secondly, as it can be seen, the weak oscillatory behaviour vanishes as $s_1/h_1$ increases, which suggests that the oscillatory behaviour in diffraction problem of SBs, especially for horizontal flat, increases as the submergence depth decreases. The physical explanation of this behaviour might relate to the diffraction wave height. As the height increases with decreasing submergence depth, for low enough $s_1$, the body is influenced (or partially influenced) by its own diffraction wave. Because the diffraction wave formation is an oscillatory function of $\exp(ix)$, it reflects itself in $CF$, $T_w$ and $R_w$. However, when $s_1$ is large enough, the body and the produced diffraction wave will not collapse and parameters like $CF$, $T_w$ and $R_w$ do not show oscillatory trends.

Figure 7 shows the formation of the diffraction wave amplitude $A_d$ alongside the breakwater's width on the horizontal flat breakwater for $\theta = 0^\circ$ and $s_1/h_1 = 0.1$ using numerical method. Firstly, $A_d$ increase with $2b/h_1$. Such an increase is much more appreciable in (a) and (b), compared to (c) and (d). Secondly, diffraction wave length decreases quickly with increasing breakwater width $b$.

Figure 8 shows the dependence of the maximum diffraction wave amplitude $|A_{d_{max}}|$ on the submergence depth $s_1$ and breakwater's width $2b$. According to Figure 7, $|A_{d_{max}}|$ occurs at $x = b$ where $A_d$ start to decrease afterwards. $|A_{d_{max}}|$ is normalised by the amplitude of the incident wave $A_i$. Figure 8 (a,b,c) present the results from the incident wave's frequency $f_i = \omega/2\pi$ of 0.2 $Hz$, 0.15 $Hz$ and 0.11 $Hz$, respectively, and the curves in each subfigure are different by changing the values of $s_1/h_1$. It can be seen that at fixed $s_1/h_1$, increasing $2b/h_1$ (breakwater's width) results in a smooth increase in $|A_{d_{max}}|/A_i$ for all incident wave frequencies. On the other hand, at fixed $2b/h_1$, as $s_1/h_1$ (the submergence depth) decreases, $|A_{d_{max}}|/A_i$ increases and the increment rate diminishes quickly from $f_i = 0.2Hz$ to $0.11Hz$. Actually, all of $s_1/h_1$ trends, almost collapse each other in $f_i = 0.11$ $Hz$. It perhaps can be expected that at very low incident wave frequencies, the curves would become flat and the amplitude $|A_{d_{max}}|$ would be independent of $s_1/h_1$.

Figure 8 (d,e,f) show the dependence of $|A_{d_{max}}|/A_i$ on $s_1/2b$. Firstly, it can be seen clearly that for a given value of $s_1/2b$, increasing $2b/h_1$, i.e. decreasing the overall water depth, would lead to diminishing $|A_{d_{max}}|/A_i$. Secondly, it is observed, especially in (e) and (f), that as $s_1/2b$ decreases to very low values, i.e. for very low submergence depth, the normalised diffraction wave amplitude $|A_{d_{max}}|/A_i$ tends to converge to a specific value $\approx 3.0$, regardless of the $2b/h_1$ value, i.e. regardless of the overall water depth at least for the range tested. Physically, the converged $|A_{d_{max}}|/A_i$ value infers zero transmission coefficient in which all incident wave energy is reflected due to high amplitudes of diffraction waves and after this point, according to the conservation of energy law, increasing the breakwater's width (or decreasing the parameter $s_1/2b$) would not results in an increase in diffraction wave amplitude any more. This result, perhaps surprisingly, shows that even for SBs, if the geometric characteristics of the body is appropriate, zero transmission coefficient can be achieved. Furthermore, the convergent value ($\approx$ 3.0) seems to be independent of the incident wave frequency. It should be noted that because of the shortcomings of the numerical method, some results in low $s_1/2b$ was not achievable (especially for Figure 8 (d)), however, the global trends show foreseeable order, reaching the convergent value of $|A_{d_{max}}|/A_i \approx 3$.

## 5. CONCLUSIONS

In this study two-dimensional SBs with rectangular cross section in finite water depth in regular waves are studied and verified for further implementation. Two new breakwaters, horizontal

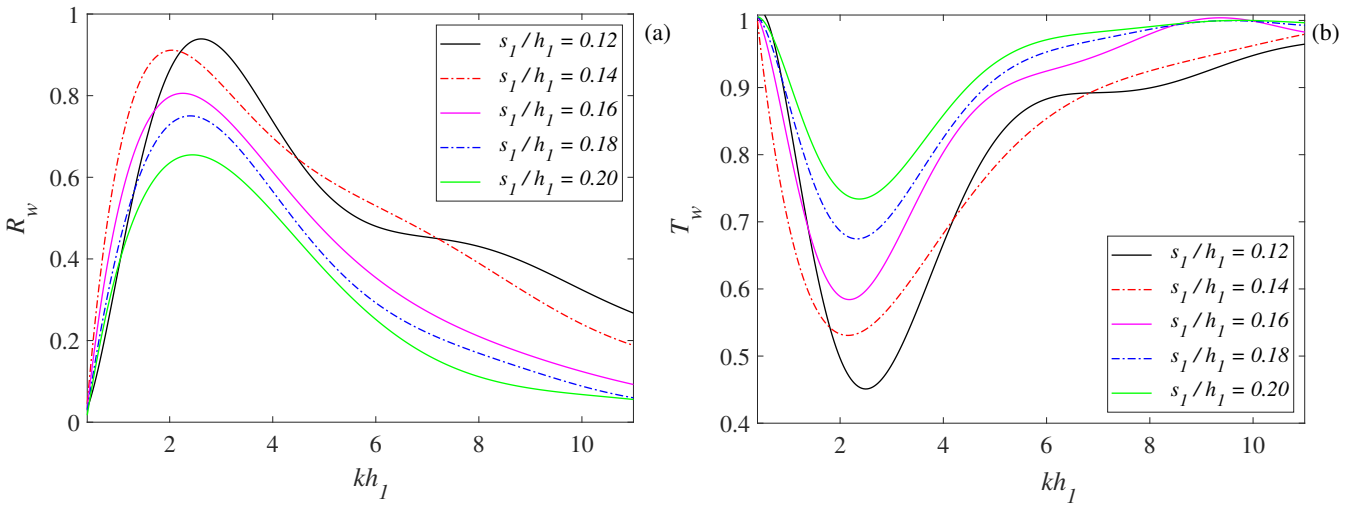


Figure 6: Reflection and transmission coefficients of horizontal flat SB in different submergence depths $\theta = 0$

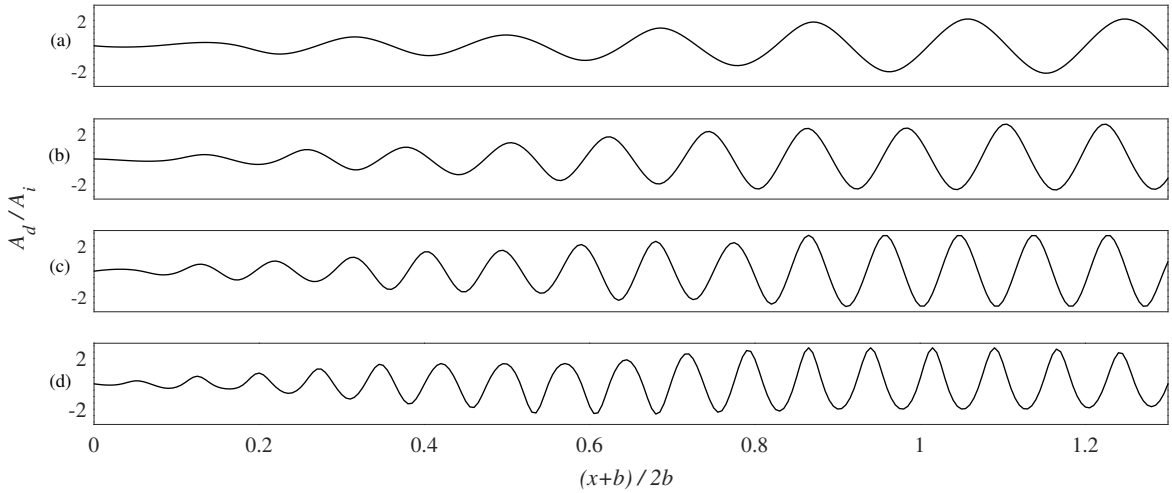


Figure 7: None-dimensional diffraction wave amplitude of horizontal flat breakwater ($\theta = 0°$, $s_1/h_1 = 0.1$) for (a) $2b/h_1 = 2$, (b) $2b/h_1 = 3$, (c) $2b/h_1 = 4$, and (d) $2b/h_1 = 5$ all in $f_i = 0.2Hz$

and vertical flat SBs of high aspect ratio, are proposed and their hydrodynamic characteristics are studied by the analytical and numerical methods. Furthermore a parametric study on the diffraction wave amplitude, which is the dominant basic parameter in breakwater's transmission coefficient, is carried out. The following conclusions can be drawn from this study:

- It is shown that the vertical flat SB produces almost no diffraction wave and transmits most of the incident wave energy. On the other hand, the horizontal flat SB shows relatively low transmission capability, which is desirable for many practical applications.

- The horizontal flat SB may be applied as an alternative to the existing breakwaters such as conventional submerged or floating breakwaters, subjected to the consideration of construction, installation and maintenance factors etc.

- Diffraction wave formation associated with the two-dimensional rectangular SBs is a decaying or a growing function of $x$, $\exp(\pm jx)$,

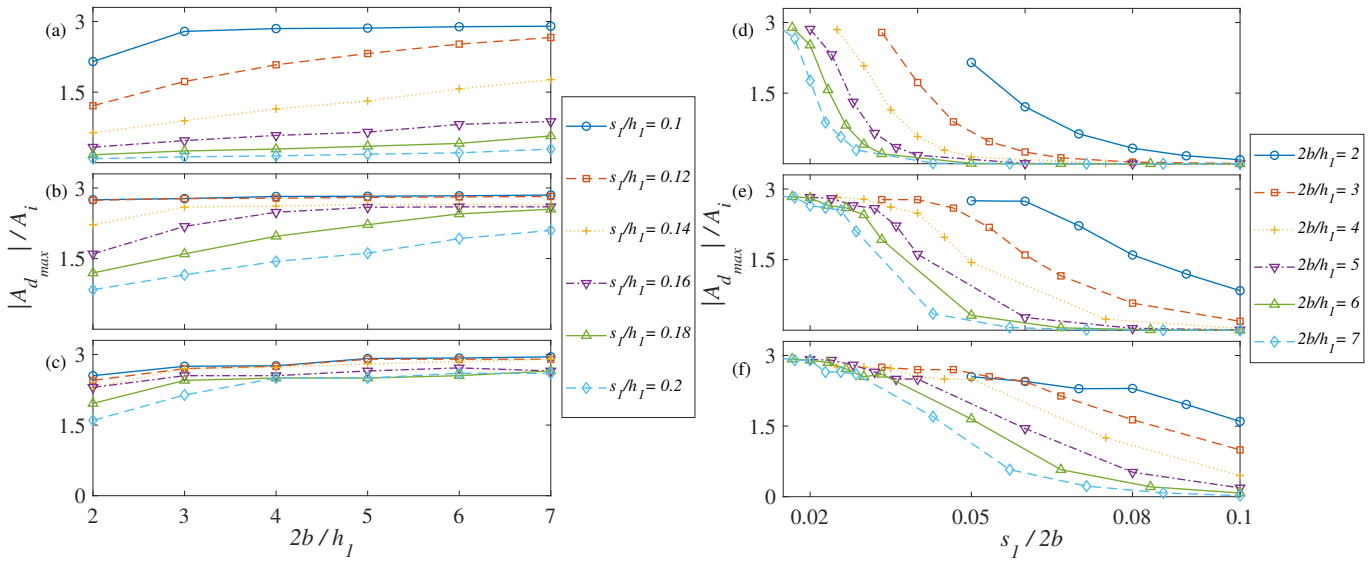


Figure 8: None-dimensional absolute maximum diffraction wave amplitude of horizontal flat breakwater ($\theta = 0°$) for $f_i = 0.2Hz$ (a,d), $f_i = 0.15Hz$ (b,e) and $f_i = 0.11Hz$ (c,f)

which reaches the maximum value at free surface and on one of the edges of the breakwater, depending on the incident wave direction. Additionally, larger breakwaters (breakwaters with high aspect ratios in the direction of incident wave) produce smaller diffraction wavelengths for a given incident wave frequency.

- Diffraction wave amplitudes tend to converge to a specific value at small submergence depth to total width ratio. This maximum amplitude corresponds to zero transmission coefficient and shows that SBs at appropriate circumstances can reflect all incident wave energy. Also, this maximum amplitude occurs at $x = b$ for $\theta = 0$ and $x = -b$ for $\theta = 180$ and seems to be independent of the incident wave frequency.

## Nomenclature

| | |
|---|---|
| $\alpha_n$ | eigenvalue of region IV |
| $\beta_n$ | eigenvalue of region II |
| $\gamma_n$ | eigenvalue of region I and III |
| $\lambda_n$ | eigenvalue of region I and III |
| $\mu_n$ | eigenvalue of region II |
| $\omega$ | Incident wave circular frequency |
| $\rho$ | Water density |
| $\theta$ | Incident wave angle to $+x$ axis |
| $\upsilon_n$ | eigenvalue of region IV |
| $\varphi_d$ | Diffraction potential |
| $\varphi_i$ | Incident wave potential |
| $\varphi_t$ | Total potential |
| $\varphi^L_{r_{2p}}$ | Particular potential for $L^{th}$ radiation motions in region II |
| $\varphi^L_{r_{4p}}$ | Particular potential for $L^{th}$ radiation motions in region IV |
| $\varphi^L_r$ | Radiation potential of the $L^{th}$ motion |
| $a$ | Breakwater height |
| $A_d$ | Diffraction wave amplitude |
| $A_i$ | Incident wave amplitude |
| $A_{d_{max}}$ | Maximum diffraction wave amplitude |

| | |
|---|---|
| $A'_{in}$ | Unknown coefficients for diffraction problem |
| $A^L_{in}$ | Unknown coefficients for radiation problem |
| $A^L_r$ | Amplitude of the $L^{th}$ motion of the body |
| $b$ | half of breakwater width |
| $c$ | Phase velocity |
| $c_g$ | Wave group velocity |
| $C_{d_u}$ | Dimensionless damping coefficient in $y$ direction |
| $C_{m_u}$ | Dimensionless added mass coefficient in $y$ direction |
| $CF_u$ | Exciting force coefficient in $u$ direction |
| $d$ | Breakwater draft |
| $E$ | Incident wave energy |
| $F$ | a $1 \times 6N$ matrix obtained from satisfying the boundary conditions between the regions |
| $F_d$ | Drift force |
| $f_i$ | Incident wave frequency |
| $F_{w_u}$ | Exciting force in $u$ direction |
| $g$ | Gravitational acceleration |
| $h_1$ | Water depth |
| $h_2$ | $(h_1 - d)$ |
| $j$ | Imaginary unit |
| $k$ | Wave number |
| $k_0$ | $ksin(\theta)$ |
| $M$ | Number of incident wave frequencies |
| $m_{L,u}$ | Added mass coefficient in $y$ direction |
| $N$ | Number of truncated series in orthogonal functions |
| $n_u$ | Generalized normal inward to the sructure |
| $N_{L,u}$ | Damping coefficient in $y$ direction |
| $P$ | Dynamic pressure |
| $R_w$ | Reflection coefficient |
| $S$ | a $6N \times 6N$ matrix obtained from satisfying the boundary conditions between the regions |
| $S_0$ | Wetted surface |
| $s_1$ | Submergence depth |
| $T_i$ | Incident wave period |
| $T_w$ | Transmission coefficient |
| $u$ | Velocity component in x direction |
| $v$ | Velocity component in y direction |
| $w$ | Velocity component in z direction |
| $X$ | a $M \times 6N$ matrix of unknown coefficients |
| $x_0$ | centroid of the breakwater in x direction |
| $y_0$ | centroid of the breakwater in y direction |
| $z_0$ | centroid of the breakwater in z direction |

## References


Abul-Azm, A., Gesraha, M., 2000. Approximation to the hydrodynamics of floating pontoons under oblique waves. Ocean Engineering 27, 365–384.

Berggren, L., Johansson, M., 1992. Hydrodynamic coefficients of a wave energy device consisting of a buoy and a submerged plate. Applied Ocean Research 14, 51 – 58.

Chen, B., Ning, D., Liu, C., Greated, C.A., Kang, H., 2016. Wave energy extraction by horizontal floating cylinders perpendicular to wave propagation. Ocean Engineering 121, 112–122.

Deng, Z., Wang, L., Zhao, X., Huang, Z., 2019. Hydrodynamic performance of a t-shaped floating breakwater. Applied Ocean Research 82, 325–336.

Garrett, C.J.R., 1970. Bottomless harbours. Journal of Fluid Mechanics 43, 433–449. doi:10.1017/S0022112070002495.

Garrett, C.J.R., 1971. Wave forces on a circular dock. Journal of Fluid Mechanics 46, 129–139.

Hsu, H.H., Wu, Y.C., 1997. The hydrodynamic coefficients for an oscillating rectangular structure on a free surface with sidewall. Ocean Engineering 24, 177–199.

Hulme, A., 1982. The wave forces acting on a floating hemisphere undergoing forced periodic oscillations. Journal of Fluid Mechanics 121, 443–463.

Kunisu, H., 2010. Evaluation of wave force acting on submerged floating tunnels. Procedia Engineering 4, 99–105.

Lee, J.F., 1995. On the heave radiation of a rectangular structure. Ocean Engineering 22, 19–34.

Li, B., Lau, S., Ng, C., 1991. Second order wave diffraction forces and run-up by finite—infinite element method. Applied ocean research 13, 270–286.

Longuet-Higgins, M.S., 1977. The mean forces exerted by waves on floating or submerged bodies with applications to sand bars and wave power machines. Proceedings of the Royal Society of London. A. Mathematical and Physical Sciences 352, 463–480.

Masoudi, E., 2019. Hydrodynamic characteristics of inverse t-type floating breakwaters. International Journal of Maritime Technology 11, 13–20.

Masoudi, E., Zeraatgar, H., 2016. Application of method of separation of variables for analyzing floating breakwater. Journal of Marine Engineering 11, 61–73.

Mohapatra, S., Soares, C.G., 2019. Interaction of ocean waves with floating and submerged horizontal flexible structures in three-dimensions. Applied Ocean Research 83, 136–154.

Sannasiraj, S., Sundar, V., Sundaravadivelu, R., 1995. The hydrodynamic behaviour of long floating structures in directional seas. Applied Ocean Research 17, 233–243.

Sannasiraj, S., Sundaravadivelu, R., Sundar, V., 2001. Diffraction–radiation of multiple floating structures in directional waves. Ocean Engineering 28, 201–234.

Tabatabaei, S.M.R., Zeraatgar, H., 2018. Parametric comparison of rectangular and circular pontoons performance as floating breakwater numerically. Polish Maritime Research 25, 94–103.

Williams, A., Lee, H., Huang, Z., 2000. Floating pontoon breakwaters. Ocean Engineering 27, 221–240.

Wu, G., 1993. Second-order wave radiation by a submerged horizontal circular cylinder. Applied Ocean Research 15, 293 – 303.

Wu, G., Taylor, R.E., 1990. The second order diffraction force on a horizontal cylinder in finite water depth. Applied Ocean Research 12, 106 – 111.

Wu, G., Taylor, R.E., 2003. The coupled finite element and boundary element analysis of nonlinear interactions between waves and bodies. Ocean Engineering 30, 387–400.

Yamamoto, T., Yoshida, A., Ijima, T., 1980. Dynamics of elastically moored floating objects. Applied ocean research 2, 85–92.

Zhan, J.m., Chen, X.b., Gong, Y.j., Hu, W.q., 2017. Numerical investigation of the interaction between an inverse t-type fixed/floating breakwater and regular/irregular waves. Ocean engineering 137, 110–119.

Zheng, Y., Liu, P., Shen, Y., Wu, B., Sheng, S., 2007. On the radiation and diffraction of linear water waves by an infinitely long rectangular structure submerged in oblique seas. Ocean engineering 34, 436–450.

Zheng, Y., Shen, Y., You, Y., Wu, B., Jie, D., 2004b. On the radiation and diffraction of water waves by a rectangular structure with a sidewall. Ocean Engineering 31, 2087–2104.

Zheng, Y., You, Y., Shen, Y., 2004a. On the radiation and diffraction of water waves by a rectangular buoy. Ocean engineering 31, 1063–1082.